TISSUE ENGINEERING: Part A
Volume 22, Numbers 13 and 14, 2016

DOI: 10.1089/ten.tea.2016.0003

termis
Tissue Engineering
& Regenerative Medicine
International Society

ORIGINAL ARTICLE

Axonal Growth Arrests After an Increased Accumulation of Schwann Cells Expressing Senescence Markers and Stromal Cells in Acellular Nerve Allografts

Louis H. Poppler, MD,[1] Xueping Ee, MD,[1] Lauren Schellhardt, BA,[1] Gwendolyn M. Hoben, MD, PhD,[1] Deng Pan, BS,[1] Daniel A. Hunter,[1] Ying Yan, MD, PhD,[1] Amy M. Moore, MD,[1] Alison K. Snyder-Warwick, MD,[1] Sheila A. Stewart, PhD,[2] Susan E. Mackinnon, MD,[1] and Matthew D. Wood, PhD[1]

Acellular nerve allografts (ANAs) and other nerve constructs do not reliably facilitate axonal regeneration across long defects (>3 cm). Causes for this deficiency are poorly understood. In this study, we determined what cells are present within ANAs before axonal growth arrest in nerve constructs and if these cells express markers of cellular stress and senescence. Using the *Thy1*-GFP rat and serial imaging, we identified the time and location of axonal growth arrest in long (6 cm) ANAs. Axonal growth halted within long ANAs by 4 weeks, while axons successfully regenerated across short (3 cm) ANAs. Cellular populations and markers of senescence were determined using immunohistochemistry, histology, and senescence-associated β-galactosidase staining. Both short and long ANAs were robustly repopulated with Schwann cells (SCs) and stromal cells by 2 weeks. Schwann cells ($S100\beta^+$) represented the majority of cells repopulating both ANAs. Overall, both ANAs demonstrated similar cellular populations with the exception of increased stromal cells ($fibronectin^+/S100\beta^-/CD68^-$ cells) in long ANAs. Characterization of ANAs for markers of cellular senescence revealed that long ANAs accumulated much greater levels of senescence markers and a greater percentage of Schwann cells expressing the senescence marker p16 compared to short ANAs. To establish the impact of the long ANA environment on axonal regeneration, short ANAs (2 cm) that would normally support axonal regeneration were generated from long ANAs near the time of axonal growth arrest (''stressed'' ANAs). These stressed ANAs contained mainly $S100\beta^+/p16^+$ cells and markedly reduced axonal regeneration. In additional experiments, removal of the distal portion (4 cm) of long ANAs near the time of axonal growth arrest and replacement with long isografts (4 cm) rescued axonal regeneration across the defect. Neuronal culture derived from nerve following axonal growth arrest in long ANAs revealed no deficits in axonal extension. Overall, this evidence demonstrates that long ANAs are repopulated with increased $p16^+$ Schwann cells and stromal cells compared to short ANAs, suggesting a role for these cells in poor axonal regeneration across nerve constructs.

Introduction

Peripheral nerve injuries are common, affecting 5% of trauma emergency visits, and cause devastating morbidity.[1] Because nerve grafts are necessary to repair a severed nerve in most cases,[2] generating an off-the-shelf nerve construct (i.e., nerve guidance conduit) that can be used to repair a variety of clinical scenarios (short gap, long gap, and small- and large-diameter nerves) has been a long-standing goal in peripheral nerve regeneration research. Acellular nerve allografts (ANAs) are a promising nerve construct because they retain native nerve tissue extracellular matrix proteins and structure facilitating axonal regeneration. In addition, ANAs and other nerve constructs that contain an internal scaffold promote superior axonal regeneration across gaps compared to ''empty'' tubes.[3] However, studies using any off-the-shelf nerve construct show that they have limited capacity for regeneration in long gap injury models (>3 cm).[4–6]

Causes of limited regeneration in long nerve constructs are poorly understood. However, recent work with long ANAs implicates cellular senescence as one underlying mechanism

[1]Division of Plastic and Reconstructive Surgery, Department of Surgery, Washington University School of Medicine, St. Louis, Missouri.
[2]Division of Cell Biology and Physiology, Washington University, St. Louis, Missouri.

of poor regenerative outcome. Our group demonstrated limited axonal regeneration across ANAs as length increased. We observed the accumulation of cells expressing senescent markers in long ANAs but were unable to establish a direct causal relationship as it is unclear whether cells expressing senescent markers were present before axonal growth arrest.[5] In addition, the contribution of other cells was not known, and the capacity of neurons to grow axons for the extended period required to cross these long ANAs has not been established.

Senescent cells arise in tissues with increasing age as well as *prematurely* in pathological conditions, such as oxidative stress, cellular overproliferation, and oncogenic signaling.[7–13] Senescence is a state of irreversible arrest of cellular proliferation frequently accompanied by altered gene and protein expression, referred to as the senescence-associated secretory phenotype (SASP).[14–16] The SASP is replete with chemokines, cytokines, growth factors, and extracellular remodeling enzymes that potentially change a regenerative environment.[7,15,17,18] While senescent cells play a role in contributing to pathologies,[15,16,18–22] they also have an essential role in tissue regeneration.[23] Senescent cells, including fibroblasts, through components of their SASP, mediate optimal wound healing in skin during injury.[23] However, in a situation of inflammation-mediated premature senescence in fibroblasts, wound healing is impaired, leading to increased scar formation.[12] These results suggest that cellular senescence has a multifaceted and context-dependent role in regeneration.

Axon regeneration depends on a complex combination of changes in the milieu of growth factors, cell adhesion molecules, and secreted molecules within injured nerve or nerve constructs.[24–29] Age-related changes to nerve, including decreased Schwann cell phagocytosis, macrophage recruitment, and growth factor expression, are associated with poor regenerative outcome.[30–32] Therefore, an accumulation of senescent cells and/or changes in cell populations within constructs could impact the regenerative process and the number of axons that cross constructs, such as ANAs.

Our previous studies identified increased numbers of cells expressing senescence markers in long ANAs after 10 weeks. Therefore, it remains unclear if senescent cells play an active role during axonal regeneration. Our current studies demonstrate the temporal relationship between cell populations, senescence markers, and axonal regeneration. We hypothesized that cells expressing senescence-associated markers precede axonal growth arrest in long ANAs and that the ANA environment is causal to axonal arrest. These studies (1) identify the temporal and spatial pattern of axonal growth in ANAs, (2) determine the cellular populations repopulating ANAs and phenotypic state preceding axonal growth arrest, and (3) demonstrate that ANAs contain an environment that causes poor axonal regeneration.

Materials and Methods

All materials were obtained from Sigma-Aldrich unless otherwise specified.

Animals and animal care

Adult male and female *Thy1*-GFP Sprague Dawley transgenic rats (200–250 g; 6–10 weeks old)[33] and adult male Lewis rats (200–250 g; 7–9 weeks old; Charles River Laboratories) were randomized to groups and underwent sciatic nerve transection and repair. At the appropriate endpoint, the animals were sacrificed for assessment of nerve regeneration within the grafts, including characterization of cellular populations, density, and functional phenotype. *Thy1*-GFP animals have axons that express green fluorescence protein to provide optical imaging capabilities to track the axonal progression after injury. Lewis ($RT\text{-}1^l$ MHC) and Sprague Dawley ($RT\text{-}1^b$ MHC) rat strains are known to be MHC incompatible for use as allograft donors.

Surgical procedures and perioperative care were performed in accordance with the Institutional Animal Studies Committee and the National Institutes of Health guidelines. Animals were fed a PicoLab Rodent Diet 20 (Purina Mills Nutrition International) and water *ad libitum*. Animals were housed in a central animal care facility and monitored daily for signs of infection or distress by trained veterinary staff.

Experimental design

Animals underwent sciatic nerve transection and grafting with a long 6-cm or short 3-cm ANA or transection without repair. A cohort of *Thy1*-GFP rats with long or short ANAs underwent serial *in vivo* imaging at 2, 4, 6, and 10 weeks to measure axonal extension. In all other *Thy1*-GFP rats, imaging at the time of tissue harvest (2 or 4 weeks) and animal sacrifice was used to indicate the furthest point of axonal regeneration and marked with a 6-0 silk suture (Ethicon). The proximal 3 cm of ANAs was divided into three even ($\sim$10 mm) segments for analysis: proximal, axonal front, and distal. These segments were analyzed for cellular populations.

A set of Lewis rats assessed the impact of the local ANA environment during axonal growth arrest (4 weeks). Axon regeneration was measured following repair of a sciatic nerve gap with standard short ANAs (2 cm) or short ''stressed'' ANAs. To generate ''stressed'' ANAs, genetically identical Lewis rats underwent sciatic transection and repair with a 6-cm ANA and were allowed to regenerate until 4 weeks. At this time, these Lewis rats were sacrificed, and a 2-cm segment of the distal portion of their long ANA was excised and used to repair new sciatic transection injuries in a second group of Lewis rats (not previously injured). The presence of cells with senescent markers in these ANAs was confirmed with senescence-associated β-galactosidase (SA-βgal) activity (details below) at the time of harvest. Axon regeneration was quantified using nerve histomorphometry, and the quantity of cell populations and senescent markers was quantified using immunohistochemistry 6 weeks after short ANA grafting.[3–5,34,35] Lewis rats that received fresh (standard) 2-cm ANAs served as a positive control.

A final set of animals assessed the impact of axonal growth arrest on neurons with two experiments. In the first experiment, *Thy1*-GFP rats with long ANAs were allowed to regenerate until 4 weeks. At this time, ANA distal to the point of axonal growth arrest ($\sim$4 cm) was excised and replaced with a fresh isograft ($\sim$4 cm). The ability of axons to resume regeneration was measured 6 weeks later using *in vivo* imaging and quantified for GFP^+ intensity. Controls for these experiments were 6-cm ANAs with sham exposure at 4 weeks but no rescue. In the second experiment, the ability of neurons to extend axons or neurites was assessed. Dorsal root ganglia

(DRG) were harvested from animals with long ANAs at 4 weeks and dissociated for neurons (culture methods follow). These ''arrested neurons'' were cultured with or without primary normal Schwann cells to measure neurite extension and compared to DRG taken from uninjured nerve (''uninjured neurons'') under similar conditions.

Surgical procedures

Surgeries were done using aseptic technique and an operating microscope (JEDMED/KAPS). Anesthesia was performed using a cocktail of ketamine (75 mg/kg; Fort Dodge Animal Health) and dexmedetomidine (0.5 mg/kg; Pfizer Animal Health). Donor nerves for ANA processing were harvested as described previously,[4] and animals were then euthanized (below). For experimental animals, the right sciatic nerve was exposed and transected 5 mm proximal to the distal trifurcation, sparing the sural nerve. The appropriate graft was sutured into the nerve gap with 9-0 nylon microsuture (Sharpoint). A two-layer closure of muscle and skin was performed using 4-0 vicryl and 5-0 nylon suture, respectively (Ethicon). At the appropriate endpoints, animals were anesthetized as before, and ANAs and nerve were excised and collected. In addition, lumbar regions L4 and L5 DRG were also collected from a set of *Thy1*-GFP Sprague Dawley rats. Following sample collection, rats were euthanized with injection of Somnasol (150 mg/kg; Delmarva Laboratories).

ANA processing

ANAs were decellularized using a series of detergents by methods described by Hudson *et al.*[36,37] In brief, the nerves were repeatedly washed in deionized water and three detergents in a sodium phosphate buffer: Triton X-100, sulfobetaine-16 (SB-16), and sulfobetaine-10 (SB-10). Triton X-100 was used in place of Triton X-200 (a discontinued product line; Dow Chemicals) as Triton X-100 at a similar concentration has been determined to effectively remove cells and proteins and reduce immunogenicity within nerve allografts.[36,38] All grafts were washed and stored in 10 mM phosphate-buffered 50 mM sodium solution at 4°C and used within 3 days.

In vivo *imaging*

Nerve grafts in *Thy1*-GFP rats were imaged intraoperatively immediately following graft implantation and at 2, 4, 6, and/or 10 weeks using methods described previously.[33] In brief, sciatic nerve was exposed and imaged using a fluorescence-enabled dissecting microscope (Olympus MVX10; Olympus America, Inc.) under GFP (488 nm) fluorescent and bright-field filters. The images were recorded monochromatically using MetaMorph version 7.1.0.0. (Universal Imaging Corporation). Images were standardized according to magnification (6.3×), exposure time (100–300 ms), and orientation. All images were standardized with respect to brightness and contrast. Distance from the proximal suture line to the distant-most point of green fluorescence and the distal suture line was measured using MetaMorph. In addition, axonal extension was normalized to graft length to account for changes in graft size over time, which is inherent to the regenerative process.[39]

Histology, histomorphometry, and electron microscopy

Histology and histomorphometric analysis were performed on long and short ANAs as well as in unrepaired, distal injured nerve as previously described.[40] Briefly, tissue was harvested and stored in 3% glutaraldehyde (Polysciences, Inc.), then postfixed in 1% osmium tetroxide, and serially dehydrated in ethanol and toluene. These tissues were embedded in epoxy (Polysciences) and sectioned on an ultramicrotome for ~1-μm cross sections. Slides were then counterstained with 1% toluidine blue dye and analyzed at 1000× on a Leitz Laborlux S microscope. Myelinated axon counts were quantified on a Leco IA32 Image Analysis System (Leco) by an observer blinded to the experimental groups.

Samples from short and long ANAs and distal unrepaired nerve harvested at 4 weeks were randomly selected for quantification of cellular populations with electron microscopy. Specimens were preserved as above and embedded in Araldite 502 resin. They were then cut into 90-nm cross sections at each 5-mm interval along the length of the graft using an LKB III microtome. Sections were stained with uranyl acetate and lead citrate. Within the area of axonal regeneration, ultramicrographs at 1500–2000× magnification were taken using a Joel 1200EX electron microscope. Cellular populations were identified by a trained histologist blinded to the experimental group from which samples were taken. Various cell types were counted per high-power field using a minimum of 10 fields per sample. Cells represented and counted included Schwann cells, stromal cells, which included fibroblasts, perineurial cells, pericytes, and mast cells, and leukocytes. Endothelial cells were insufficiently represented to base comparisons between groups but counted to determine the total cell number. The total number of cells per field were normalized to the field area (density) to standardize counts for appropriate comparisons between groups.

Immunohistochemistry

Immunohistochemical (IHC) staining was used to identify cell populations and cellular state (senescence) within the area of axonal regeneration. ANAs were harvested and divided as described in the experimental design, including normal nerve and distal injured nerve as control. All tissues were explanted and immediately placed in 4% paraformaldehyde in phosphate-buffered saline (PBS) for 8–12 h and then moved to 30% sucrose in PBS solution for 24–48 h. Samples were then frozen in OCT Compound (VWR) and cut as longitudinal 20-μm-thick sections onto pretreated charged glass slides. Sections were rehydrated with PBS and blocked using 2% normal goat serum and 0.5% bovine serum albumin before primary antibody staining. Primary antibody in blocking buffer (above) was applied and incubated at 4°C overnight with antibodies outlined in Table 1. Sections were then washed in PBS and stained for the appropriate fluorochrome-conjugated secondary antibodies for 1 h at room temperature. All sections were mounted with Fluoroshield mounting medium with DAPI (Abcam) and then imaged using the NanoZoomer HT (Hamamatsu) at overall 200× magnification or a Fluoview FV1000 confocal microscope and acquisition system (Olympus) at overall 600× magnification (60× oil immersion objective). A minimum of three sections were analyzed and averaged for each

Table 1. Immunohistochemistry Markers Used to Identify Cellular Populations and Senescence

Protein marker	*Target/function*	*Primary antibody*	*Catalog number*	*Dilution factor*
S100β	Schwann cells	Polyclonal Rabbit Anti-S100β (Dako)	Z0311	1:500
CD90	Fibroblasts, endothelial cells, T cells, and NK cells	Monoclonal Mouse Anti-CD90/ Thy1 (Abcam)	AB225	1:1000
Fibronectin	Endoneurial cells (stromal cells)	Polyclonal Goat Anti-Fibronectin (Santa Cruz Biotechnology)	SC-6952	1:100
CD68	Macrophages	Monoclonal Mouse Anti-CD68 [ED1] (Abcam)	AB31630	1:100
p16	Cell cycle regulator	Monoclonal Mouse Anti-CDKN2A/ p16INK4a (Abcam)	AB54210	1:250
p53	Cell cycle regulator	Monoclonal Mouse Anti-p53 (Abcam)	AB26	1:250
Ki67	Cellular proliferation marker	Polyclonal Rabbit Anti-Ki67 (EMD Millipore)	AB9260	1:300

tissue area using ImageJ (NIH). For intensity analysis, normal nerve was always included for sample staining as a control and for normalization of staining intensity. For cell counts, field size was kept standard at a 60× objective (600× magnification overall), and colocalization of the primary marker(s) with DAPI was considered a positive cell.

Histochemical analysis of senescence (SA-βgal)

SA-βgal staining was performed on ANAs immediately following harvest. Samples were flash frozen in OCT Compound (VWR) on liquid nitrogen and sectioned as longitudinal 20-μm-thick slices collected on glass slides. All areas within the epineurium of the nerve/ANA were assessed for SA-βgal activity. The Senescence Detection Kit (Abcam) was used according to the manufacturer's protocol. Control nerve (normal uninjured nerve) was always included during staining. Sections were imaged at 20× magnification using the NanoZoomer HT. To compare staining between groups, the average staining intensity was measured from normal nerve using ImageJ (NIH). Senescent cells and the area they occupied were defined positive if SA-βgal activity was at least two standard deviations greater than the average staining intensity for normal uninjured nerve. The total area of positive staining was normalized to the total area of the ANA and reported as a percentage of the tissue area positive for SA-βgal activity.

Neurite extension assay

DRG harvested from animals following axonal arrest within long ANAs were dissociated to obtain neurons. These neurons were compared to those without injury or axonal arrest. To obtain neurons from DRG, DRG following excision were digested and minced in 0.125% collagenase (195 U/mg; Worthington) and 0.05% dispase (Worthington) at 37°C for 75 min. Following enzyme solution removal, the DRG were further digested in 0.05% trypsin (Gibco) at 37°C for 20 min. A 70-μm strainer (VWR) was used to strain the cell solution, followed by cell resuspension in Dulbecco's modified Eagle's growth medium (DMEM) supplemented with 10% heat-inactivated fetal bovine serum, 100 U/mL penicillin, 100 μg/mL streptomycin, and 0.25 μg/mL amphotericin B. Cells were then plated at 2000 cells per well either alone or on top of existing SC cultures (below) and allowed to extend neurites for 48 h. Five wells per group were prepared. Finally, 10–20 neurons per well were randomly selected and photographed at 10× under an FITC (488 nm) filter (Omega Optical) on an Olympus IX81 microscope using Micro-Manager v1.4.[41] The longest neurite extension from the cell body and the number of branching points were measured using ImageJ.[42]

To obtain SCs, the uninjured sciatic nerve of Lewis rats was incubated in DMEM (Invitrogen) supplemented with 10% heat-inactivated fetal bovine serum, 100 U/mL penicillin, 100 μg/mL streptomycin, 0.25 μg/mL amphotericin B, 20 μg/mL bovine pituitary extract (Biomedical Tech, Inc.), and 5 μM forskolin for 7 days.[43–45] These nerves were then placed in growth medium with 1.25 U/mL dispase (Worthington) and 0.5% collagenase IV (Worthington) at 37°C for 8–12 h. Next, digested nerves were strained and centrifuged at 400 *g* for 6 min to collect the cell component. Cells were then cultured on poly-L-lysine (pLL)-coated tissue culture dishes (BD Falcon) for 6 days. At this time, fibroblasts were complement killed with anti-Thy 1.1 antibody (1:40 dilution in media; Serotec) and rabbit complement (1:4 dilution in media). All cultures were performed at 37°C in a water-jacketed incubator at 5% CO_2 and 20% O_2. SCs were seeded on pLL-coated 24-well plates (Corning) at a density of 40,000 cells per well (100% confluency) and allowed to adhere for 24 h before neuronal plating. SC status (i.e., lack of senescence markers) was confirmed in this primary culture.

Statistical analyses

IBM SPSS version 22 was used for all statistical analyses. All data were compiled as mean ± standard deviation. Data were tested for normality graphically and using the Kolmogorov–Smirnov test. ANOVA was used to test differences between groups with the primary comparison of interest specified a priori and *post hoc* comparisons with Tukey's test. When two groups were compared, a *t*-test was performed. A significance level of $p < 0.05$ was used in all statistical tests performed.

Results

Axonal regeneration arrests by 4 weeks in long (6 cm) ANAs, while axons cross short (3 cm) ANAs

To identify the time of axonal growth arrest, we used the *Thy1*-GFP rat to serially track axonal regeneration in short (3 cm) and long (6 cm) ANAs over a 10-week period with live optical imaging (Fig. 1A–D). Axons advanced 6.5 ± 1.8 mm in the long ANAs for $\sim$4 weeks. However, after 4 weeks, axonal extension was unchanged for the remaining 6 weeks (''arrested''). In contrast, axons regenerated approximately the same distance within short ANAs by 4 weeks and continued to regenerate after 4 weeks, where axons reached the distal nerve by 10 weeks achieving successful regeneration across the short ANA (Fig. 1E). As constructs contracted as time progressed[39] for both ANAs, axonal extension measurements were also normalized to the ANA length (Fig. 1F). This analysis revealed the same conclusions. In addition, both analyses revealed that axons failed to advance even 3 cm within a long ANA. As axonal growth arrested in long ANAs by 4 weeks, differential analyses between these grafts to short ANAs at 4 weeks could identify potentially causal factors involved in axonal growth arrest.

Peripheral nerve support cells repopulate short and long ANAs

Normally, Schwann cells, stromal cells, such as fibroblasts, and macrophages comprise the majority of cells in normal and injured nerve.[46–49] While Schwann cells and macrophages have specific cellular markers, nerve stromal cells, such as fibroblasts, perineurial cells, pericytes, and mast cells, are typically identified through exclusion from other cells ($S100^-/CD68^-$) and association with fibronectin and/or collagen.[48,50,51] Differential assessment of these cellular populations within the ANAs (within the epineurial shealth) was performed by comparing the short ANAs (3 cm) to the proximal 3 cm of long ANAs at 4 weeks as long ANAs still contain axons within this portion of the ANA. Before graft excision, the area of the axonal front was indicated using live imaging, and ANAs were divided into three even ($\sim$10 mm) segments for analysis: proximal, axonal front, and distal (Fig. 2A).

IHC staining for protein markers expressed by neural support cells was used to first screen spatial segments. S100β (Schwann cell; Fig. 2B), CD90 (fibroblasts, endothelial cells, T cells, and NK cells; Fig. 2C), and CD68 (macrophage; Fig. 2D) mean intensities were generally similar between short and long ANAs. A notable exception was CD90 mean intensity, which was increased twofold to injured nerve by both short and long ANAs, suggesting an increased presence of stromal cells, such as fibroblasts, in either ANA (Fig. 2C). In addition, long ANAs demonstrated $\sim$1.4-fold greater CD68 intensity compared to short ANAs in their distal segment, suggesting differential repopulation of macrophages (Fig. 2D). Overall, the IHC mean intensity screen demonstrated that ANAs were repopulated by the major support cells of nerve.

Based on the screen, the total cell density and individual cell populations were quantified. As the total cell density did not differ between long or short ANAs (Fig. 3A), we considered the percentage of Schwann cells ($S100\beta^+$), stromal cells ($fibronectin^+/S100\beta^-/CD68^-$), and macrophages ($CD68^+$). Schwann cells represented the majority in either long or short ANAs.

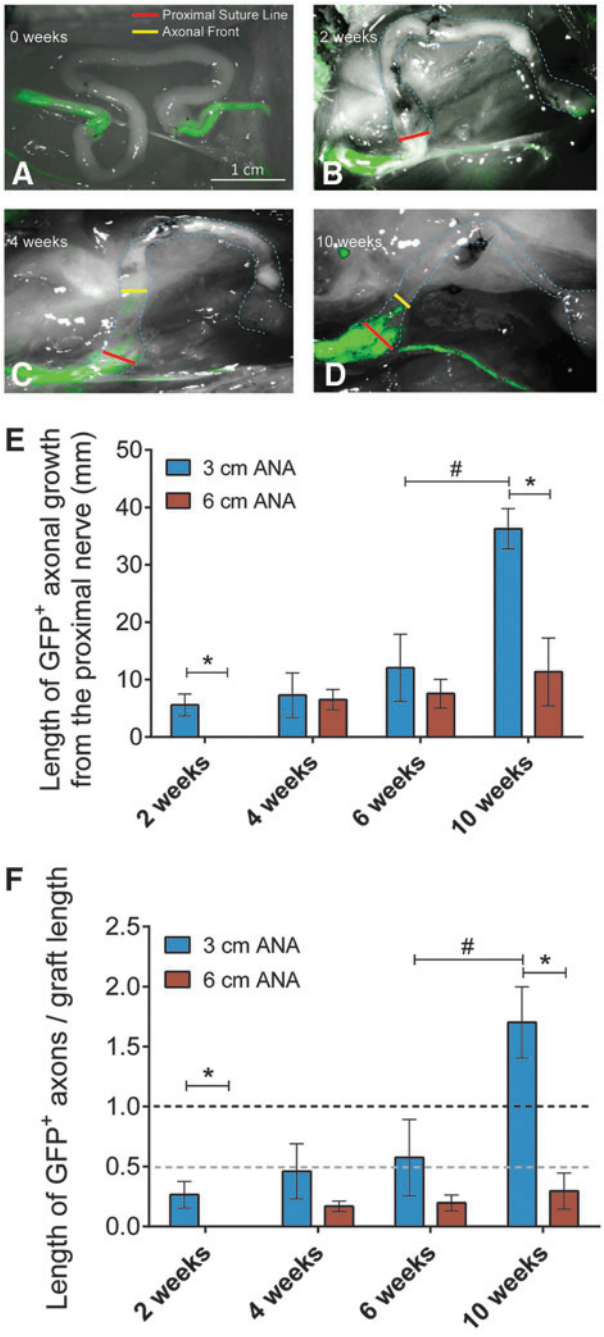

FIG. 1. Axonal regeneration within ANAs. *Thy1*-GFP rats were used to measure axonal growth through ANAs (*red line* start of ANA; *dashed line* outlines ANA) over the time course of 10 weeks, where the axonal front was used to measure the distance axons extended (*yellow bar*). **(A–D)** Representative images of optical macroscopic imaging of GFP axons regenerating through long 6-cm ANAs. **(E, F)** Axon growth into 6-cm ANAs is delayed relative to 3-cm ANAs (2 weeks), and the axonal front does not change after 4 weeks (axonal growth arrest). Axons continue to advance in 3-cm ANAs without arresting their growth. Means with standard deviation are represented, $n = 4$ per group; * represents statistical significance between 6-cm versus 3-cm ANAs, and # indicates statistical significance between ANAs at different times ($p < 0.05$). *Dotted lines* represent either the end (*black*) or halfway (*gray*) point of ANAs. ANAs, acellular nerve allografts. Color images available online at www.liebertpub.com/tea

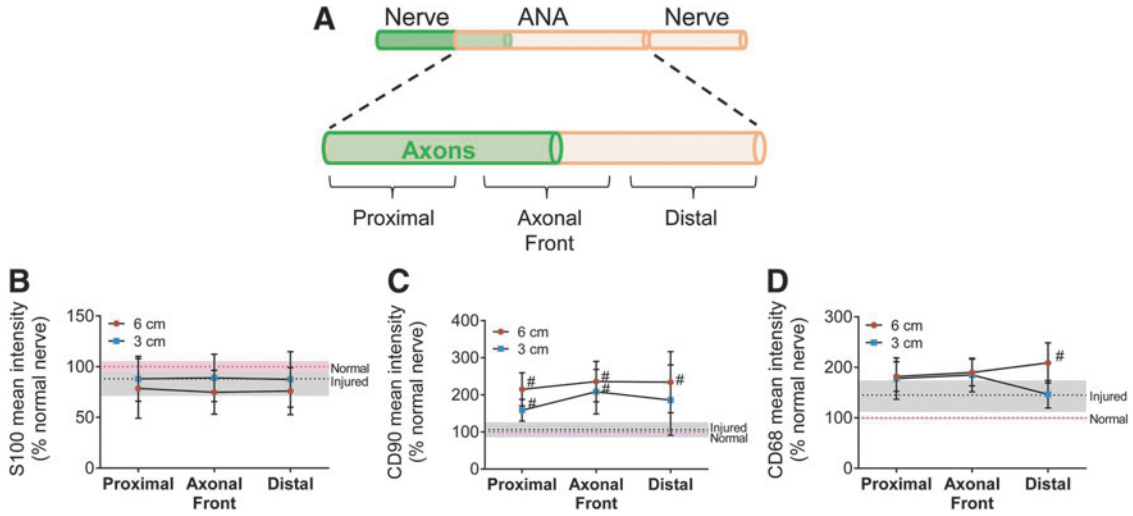

FIG. 2. Assessment of cellular population marker intensity within ANAs. **(A)** The area of the axonal front was indicated using live imaging in *Thy1*-GFP rats at 4 weeks, and ANAs were divided into three approximately even (10 mm) segments for analysis: proximal, axonal front, and distal. Unrepaired, transected, distal nerve and normal uninjured nerve served as controls. **(B–D)** Mean intensity for expressed proteins revealed the presence of Schwann cells (S100β), stromal cells (CD90), and macrophages (CD68). CD90 was elevated relative to injured and normal nerve for either ANA length. Means with standard deviation are represented, $n = 4$ per group; *pink* and *gray dashed lines* and *shading* are mean and standard deviation for normal and injured nerve, respectively. # Indicates statistical significance between either ANA versus injured nerve ($p < 0.05$). Color images available online at www.liebertpub.com/tea

While the percentage of Schwann cells did not vary between long or short ANAs (Fig. 3B), the percentage of stromal cells was increased in long ANAs (Fig. 3C). The percentage of macrophages did not differ within the axonal front or distal segments (Fig. 3D) despite differences in the previous intensity analysis. As stromal cells increased in both the axonal front and distal segment of long ANAs, these data suggest that these cells may play a role in axonal regeneration and growth in ANAs.

To further elucidate IHC characterization of cell populations, differential histological analysis of the axonal front segment at 4 weeks was also performed. We relied on morphological characteristics as opposed to protein markers, which may change based on cell phenotype (Fig. 4A). Again, Schwann cells represented the majority of cells within ANAs and did not differ between long and short ANAs (Fig. 4B). In this analysis, the percentage of stromal cells, such as fibroblasts, represented the second most represented cell in either ANA and did not differ between long and short ANAs. These data taken together with the IHC characterization of cell populations suggest that Schwann cells and stromal cells (particularly ones associated with fibronectin) likely play roles in ANAs due their predominant presence.

Cellular senescence markers have accumulated during axonal growth arrest in long ANAs

To understand why axon regeneration arrests in long but not short ANAs, we considered phenotypic changes to the

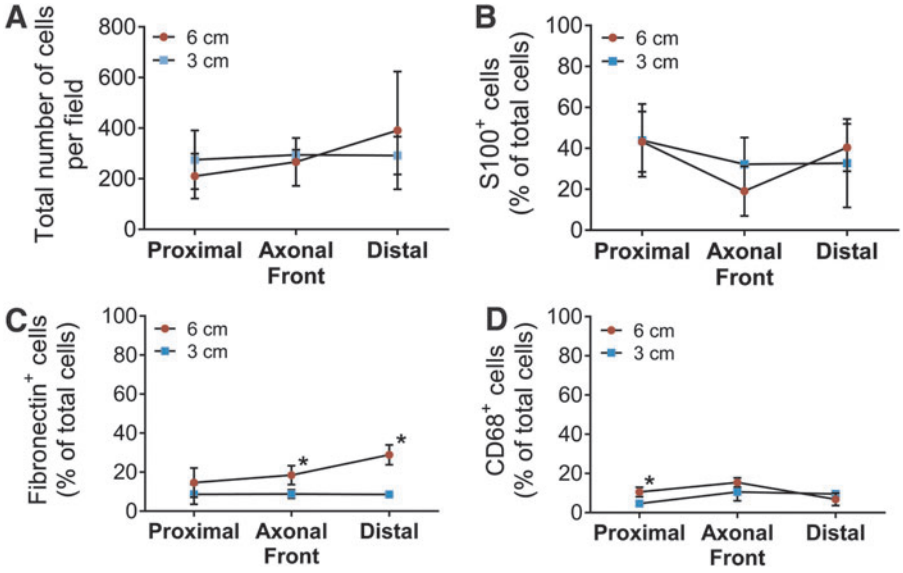

FIG. 3. Assessment of cellular populations within ANAs using immunohistochemical staining. Spatial areas within ANAs (Fig. 2A) were assessed for cell populations. The total cell density **(A)** between either ANA did not differ. The composition of the total cell population is represented for the percentage of Schwann cells (S100β; **B**), stromal cells (fibronectin$^+$/S100β$^-$/CD68$^-$; **C**), and macrophages (CD68; **D**). Means with standard deviation are represented and $n = 4$ per group. * Indicates statistical significance between 6-cm versus 3-cm ANAs ($p < 0.05$). Color images available online at www.liebertpub.com/tea

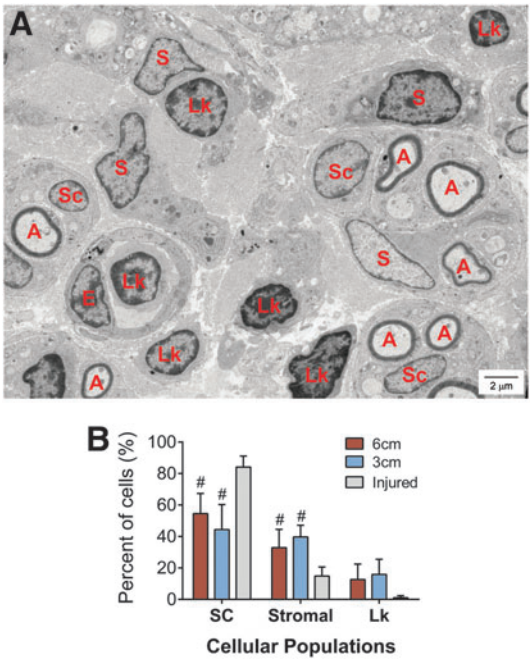

FIG. 4. Assessment of cellular populations within ANAs using histology. The area of the axonal front (Fig. 2A) was assessed using histology to identify cellular composition within ANAs. **(A)** Representative electron micrograph of histological section of 3-cm ANA, where A, myelinated axons; SC, Schwann cell; S, stromal cell; Lk, leukocyte; E, endothelial cell (which were not quantified due to insignificant representation in electron microscopy images). **(B)** The composition of the total cell population is represented for the percentage of Schwann cells, stromal cells, and leukocytes. Means with standard deviation are represented, $n=4$ per group, and # indicates statistical significance to injured nerve ($p<0.05$). Color images available online at www.liebertpub.com/tea

cells repopulating the constructs. Senescent cells can be characterized by increased SA-βgal[52–55] and increased expression of cell cycle regulators (p16 and/or p53).[14,15] At the time of axon regeneration arrest, the percent area of ANAs positive for SA-βgal activity was greater in long ANAs than in short ANAs in all spatial segments (Fig. 5A, B), suggesting a greater accumulation of senescent cells. We also screened these tissue segments using IHC mean intensity for cell cycle regulators and proliferation markers. Mean intensity of cellular proliferation marker Ki67 (Fig. 5C) or cell cycle regulator p53 (Fig. 5D) was not different between ANAs. However, p16 was elevated in both long and short ANAs compared to normal and injured nerve (Fig. 5E), suggesting cells may be undergoing arrest through the p16 pathway (as opposed to the p53 pathway).

Based on the IHC screen, the percentage of Schwann cells ($S100\beta^+$) and stromal cells (fibronectin$^+$) expressing p16 (colocalization) was quantified. While we previously did not find differences in the percentage of Schwann cells between either ANA (Fig. 3B), the percentage of Schwann cells colocalized with p16 was increased in long compared to short ANAs (Fig. 6A). Conversely, the percentage of stromal cells colocalized with p16 did not differ between either ANA (Fig. 6B). Overall, the data demonstrate that long ANAs accumulate greater levels of senescent markers with a prominent increase in the ratio of Schwann cells colocalized with p16, suggesting an increase in Schwann cells undergoing stress and/or senescence.

The cellular composition of long ANAs before axonal growth arrest reflects similar trends to the composition near the time of axonal growth arrest

To establish the presence of increased levels of prematurely senescent and/or stromal cells before axonal arrest, long ANAs

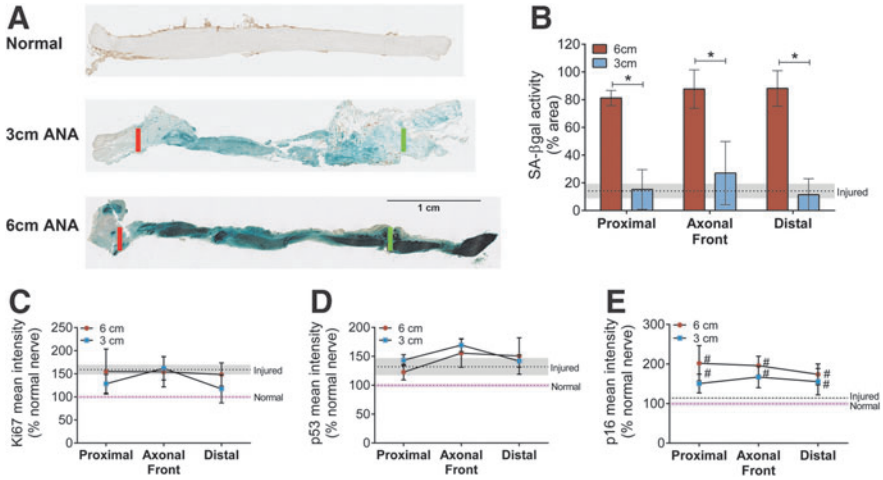

FIG. 5. Assessment of cellular senescence markers within ANAs. **(A)** Representative images of SA-βgal (*blue/dark* staining) activity taken from longitudinal sections of 3-cm (*top*) and 6-cm (*bottom*) ANAs at 4 weeks. *Red line* indicates proximal suture line, and *green line* indicates end of 3-cm ANA or proximal half (3 cm) of 6-cm ANA. Spatial areas within ANAs (Fig. 2A) were assessed for senescence markers. **(B)** Positive SA-βgal activity was measured as a percentage of the tissue area in 3- and 6-cm ANAs. Mean intensity of cell proliferation (Ki67; **C**) and cell cycle regulators (p53; **D,** p16; **E**) demonstrates elevated p16 relative to normal and injured nerve. Means with standard deviation are represented, $n=4$ per group; *pink* and *gray dashed lines* and *shading* are mean and standard deviation for normal and injured nerve, respectively. * Indicates statistical significance between 6-cm versus 3-cm ANAs, and # indicates statistical significance between either ANA versus injured nerve ($p<0.05$). SA-βgal, senescence-associated β-galactosidase. Color images available online at www.liebertpub.com/tea

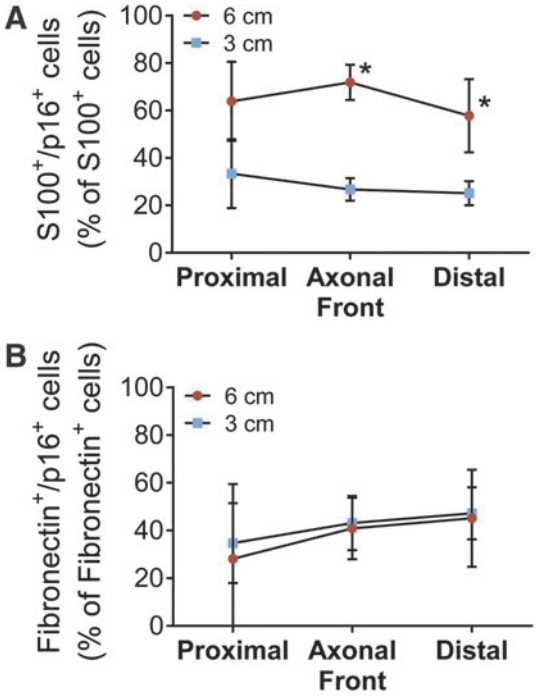

FIG. 6. Assessment of cell populations expressing senescence markers within ANAs. Spatial areas within ANAs (Fig. 2A) were assessed for cell populations colocalized with senescence markers. The percentage of Schwann cells ($S100\beta^+$ cells) colocalized with p16 **(A)** is increased in long compared to short ANAs, while that of stromal cells (fibronectin$^+$ cells) colocalized with p16 **(B)** is not different for either ANA. Normal nerve contained less than 5% $p16^+$ cells (data not shown). Means with standard deviation are represented, $n=4$ per group, and * indicates statistical significance between 6-cm versus 3-cm ANAs ($p<0.05$). Color images available online at www.liebertpub.com/tea

at 4 weeks were compared to those at a 2-week endpoint. At 2 weeks, long ANAs had similar percentages of Schwann cells and macrophages, but there was a substantial increase in the percentage of stromal cells (fibronectin$^+$/S100β^-/CD68$^-$) (Fig. 7A–C). SA-βgal activity was similarly elevated at 2 and 4 weeks compared to injured nerve (Fig. 7D). Proportions of Schwann cells (Fig. 7E) and stromal cells (Fig. 7F) expressing p16 were similar at 2 and 4 weeks. Overall, the data suggest that increased stromal cells and $p16^+$ Schwann cells play a role in axonal growth arrest in ANAs.

The long ANA environment at 4 weeks limits axonal regeneration

The impact of long ANAs on axonal regeneration was further elucidated by generating short ANAs (2 cm; ''stressed'') taken from long ANAs (6 cm) 4 weeks following their initial implantation (Fig. 8A). Using short constructs (<3 cm), axonal regeneration across stressed ANAs is anticipated if the ANA environment is not a major factor. While generating these stressed ANAs, SA-βgal activity was confirmed, where results mirrored previous findings (data not shown). At 6 weeks following retransplantation, the ''stressed'' ANAs were assessed for cellular compositions and compared to normal short ANAs (2 cm; ''standard''). Both stressed and standard ANAs contained similar total cell densities (Fig. 8B) as well as a similar percentage of Schwann cells (Fig. 8C), which represented the majority of cells. The percentage of Schwann cells expressing p16 ($S100^+/p16^+$) was increased in stressed ANAs compared to standard ANAs (Fig. 8D), while there were no differences in the percentage of stromal cells (fibronectin$^+$) in either ANA (data not shown). Comparing axonal regeneration across these ANAs, axons regenerated across standard ANAs in all animals by 6 weeks, where quantitative histological

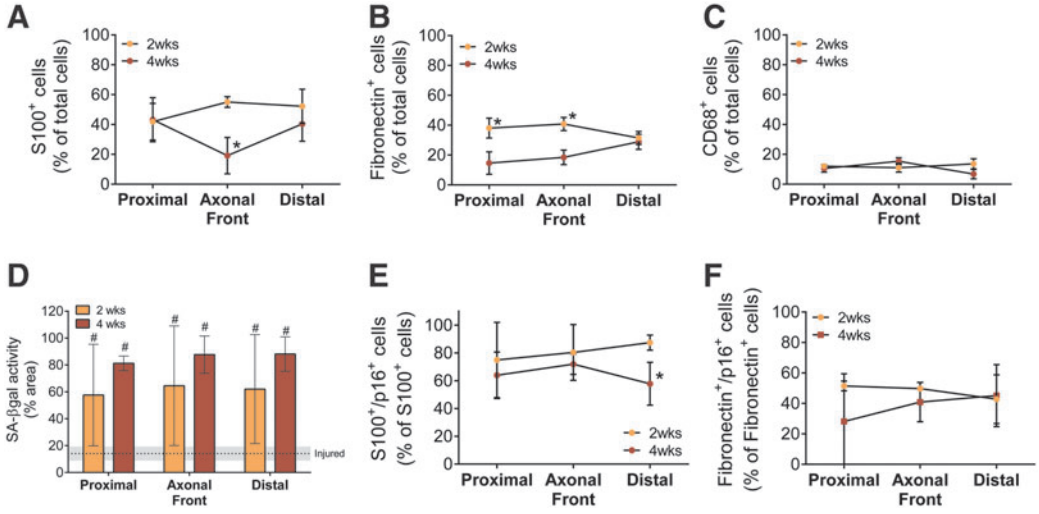

FIG. 7. Assessment of cellular populations and senescence markers within long ANAs at 2 and 4 weeks. Spatial areas within long ANAs were assessed at 2 and 4 weeks (Fig. 2A). The percentage of stromal cells (fibronectin$^+$/S100β^-/CD68$^-$) was substantially increased at 2 weeks compared to 4 weeks **(B)**, while Schwann cells (S100β; **A**) and macrophages (CD68; **C**) had few differences. **(D)** SA-βgal$^+$ activity area is greater than injured nerve at 2 weeks, where unrepaired, transected, distal nerve and normal uninjured nerve served as controls. The percentage of Schwann cells colocalized with p16 **(E)** is elevated at 2 weeks, while that of fibroblasts colocalized with p16 **(F)** is not different from 4-week patterns. Means with standard deviation are represented and $n=4$ per group. * Indicates statistical significance between 6-cm versus 3-cm ANAs, and # indicates statistical significance between either ANA versus injured nerve ($p<0.05$). Color images available online at www.liebertpub.com/tea

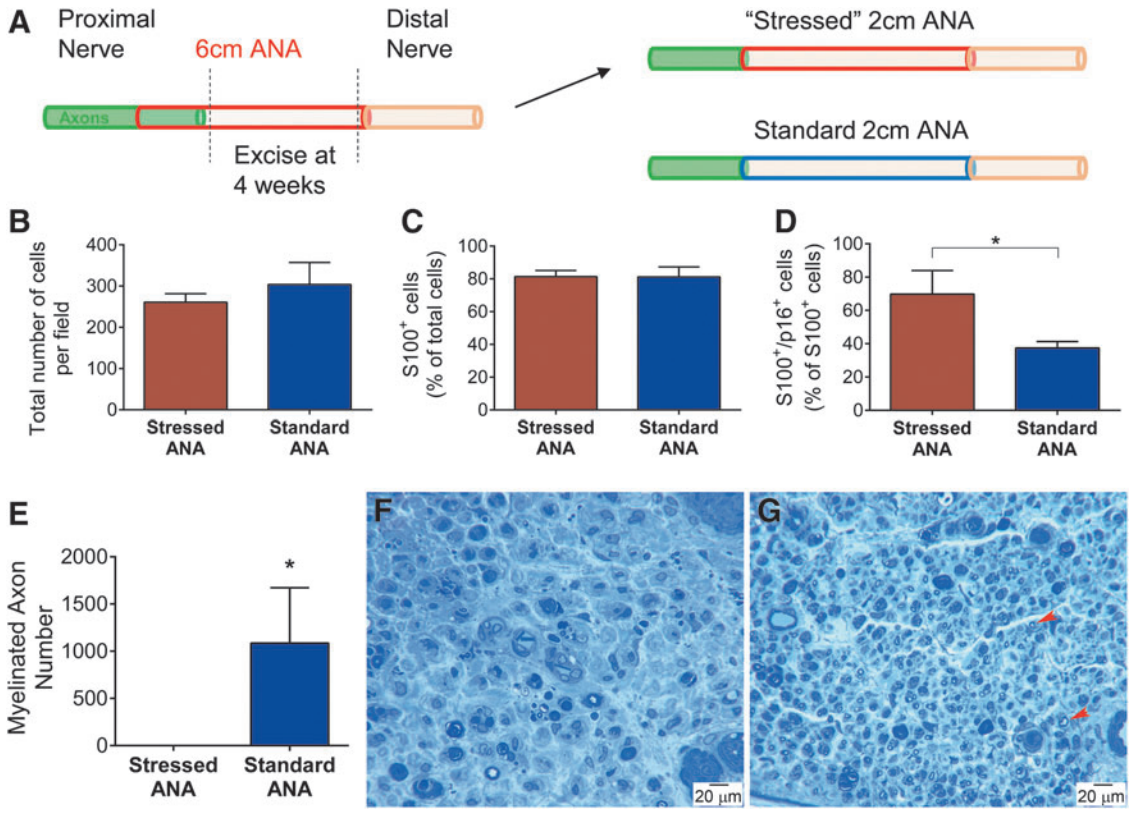

FIG. 8. Assessment of the regenerative potential of long ANAs following axonal growth arrest. **(A)** Diagram depicting how short ANAs (stressed) were derived from long ANAs 4 weeks following initial long ANA implantation. At a 6-week endpoint, nerve grafts and distal nerve were assessed for regeneration and cell populations. Groups had similar cell densities **(B)** and percentages of Schwann cells (S100β; **C**), but an increased percentage of $S100\beta^{+}/p16^{+}$ cells in stressed ANAs compared to standard ANAs **(D)**. **(E)** Histomorphometric analysis of myelinated axon counts between standard and stressed ANAs. Histological micrographs of nerve cross sections distal to the grafts [stressed **(F)** and standard **(G)** ANA groups]. Representative myelinated axons are indicated with *red arrows*. Means with standard deviation are represented, $n = 3$ per group, and * represents statistical significance ($p < 0.05$). Color images available online at www.liebertpub.com/tea

measures demonstrated robust myelinated axon counts (Fig. 8E, G). Conversely, no axons regenerated across ''stressed'' ANAs in any animal (Fig. 8F). Therefore, the data demonstrate that the long ANA environment is deleterious to axonal regeneration.

Replacement of the long ANA region distal to arrested axons "rescues" axonal regeneration across the long gap

The impact of removing the deleterious ANA environment on axon regeneration was evaluated by two sets of experiments. In the first, a fresh isograft (~4 cm) was used to replace the distal end of the long ANA near the area of axonal growth at 4 weeks (Fig. 9A). Previously, we determined that 4-cm isografts contain significantly less stromal cells and senescent markers compared to 4-cm ANAs.[5] All animals receiving this isograft ''rescue'' regenerated axons across the 4-cm isograft to cross the entire 6-cm gap. Without removal and replacement of the ANA distal to axons, axonal regeneration did not proceed. In the second experiment, DRG were harvested from nerve receiving long ANAs at 4 weeks and dissociated for neurons (''arrested neurons''). These ''arrested neurons'' were cultured to measure neurite extension and compared to DRG taken from uninjured nerve (''uninjured neurons''). With or without normal cultured Schwann cells to encourage neurite extension, ''arrested neurons'' extended longer neurites than uninjured neurons (Fig. 9B). The data suggest that components within long ANAs cause axonal growth arrest as neurons are capable of regenerating and extending axons after growth arrest.

Discussion

The current experiments demonstrate that prematurely senescent cells are present *before* and *during* axonal growth arrest in ANAs, which were placed in young rats where senescent cells are not normally present.[21] These studies suggest that an increased accumulation of stromal cells ($fibronectin^{+}/S100\beta^{-}/CD68^{-}$) and senescent Schwann cells within long ANAs impacts axonal regeneration across ANAs. We also further demonstrate that axonal extension and regeneration are dependent on the environment within ANAs as short ''stressed'' ANAs derived from long ANAs do not promote axonal regeneration.

The initial microenvironment of any acellular tissue construct, including ANAs, differs from denervated distal nerve or auto/isografts in key ways, most notably cells.[56,57] A variety of techniques have been used to generate acellular constructs, including repeated freeze–thaw cycles,

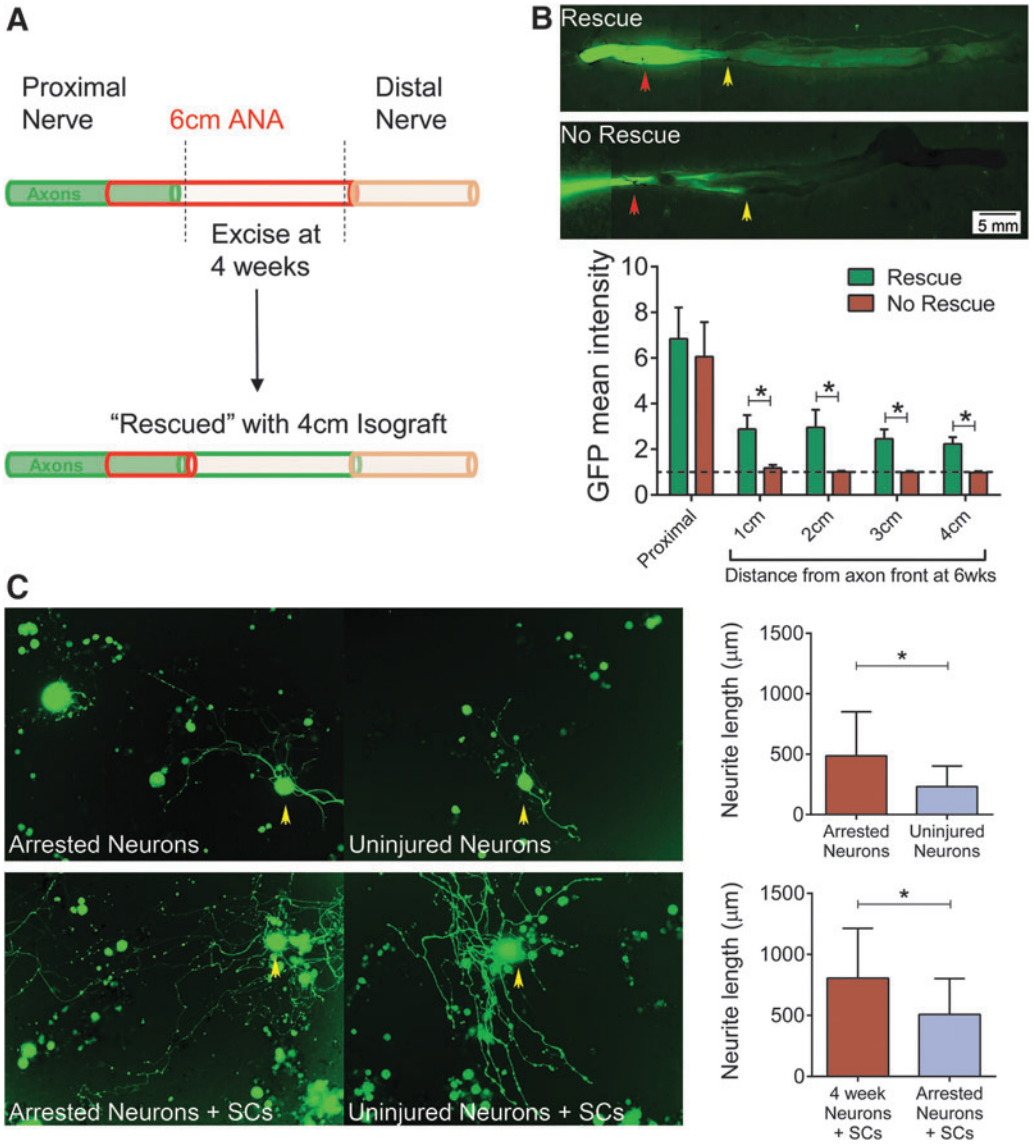

FIG. 9. Assessment of the regenerative potential of neurons following axonal growth arrest. Long ANAs were replaced with long isografts (''rescue'') at the area of axonal growth arrest at 4 weeks (diagram; **A**). **(B)** Representative images of nerve taken from a *Thy1*-GFP rat demonstrate axonal extension (*green*) into the long isograft (rescue) or without rescue ($n=4$ per group). *Red arrow* indicates the proximal portion containing the original 6-cm ANA, and *yellow arrow* indicates the point of axonal front before isograft placement. Analysis of GFP intensity between rescue and no-rescue groups revealed increased GFP intensity in rescue spatial regions. **(C)** Neurons derived from nerve receiving long ANAs were harvested from DRG at 4 weeks after axonal growth arrest. ''Arrested neurons'' were cultured with or without Schwann cells: Micrographs of neurite extension from these neurons with *yellow arrows* indicating representative neurons. Neurite extension length was significantly greater for arrested neurons compared to naive/uninjured nerve-derived neurons ($n>50$ per group). Means with standard deviation are represented, and * represents statistical significance ($p<0.05$). DRG, dorsal root ganglia. Color images available online at www.liebertpub.com/tea

exposure to radiation, lyophilization, extended storage in cryopreservation solution, and currently employed detergent processing.[4,6,37,57–61] While the failure of axons to cross long nerve constructs is a well-established issue, previous efforts using freeze-dried grafts reported difficultly with Schwann cell repopulation ($S100^+$) and migration within long grafts.[6,58,62–65] Therefore, failure of axonal regeneration was more likely an issue of insufficient support cells to allow axonal advancement. Our findings demonstrate that detergent-processed ANAs regardless of length are robustly repopulated with support cells, including Schwann cells and stromal cells, such as fibroblasts, within weeks of implantation.

We found an increase in stromal cells (fibronectin$^+$/S100β$^-$/CD68$^-$) in long compared to short ANAs, suggesting a possible cause for regenerative differences between these ANA lengths. As histological assessment of stromal cell numbers did not demonstrate differences in long and short ANAs, these results suggest that a particular subpopulation of stromal cell is accumulating in long ANAs, such as activated fibroblasts, which are associated with fibronectin.[51,66] Therefore, further study to elucidate the role of

stromal cell subpopulations will be needed. An additional explanation for poor axonal regeneration is suggested by our other major finding: Schwann cells expressing p16 (a senescence marker). Poor regenerative outcomes are associated with age-related changes to nerve, including decreased Schwann cell phagocytosis, macrophage recruitment, and growth factor expression.[30–32] Therefore, the premature onset of cellular senescence within a range of cells repopulating nerve constructs could have an impact on regenerative outcomes. Our results strongly suggest that Schwann cells exhibiting markers of stress and/or senescence impact axonal regeneration as all analyses identified this cell associated with poor regenerative outcomes.

Markers of cellular senescence were shown to be significantly elevated in long ANAs at the area of axonal growth arrest both before and just before axonal growth arrest. This result was in stark contrast to short ANAs. Short ANAs contained significantly reduced numbers of cells expressing senescent markers and facilitated axons across the construct. The association of cells expressing senescence markers in both short and long ANAs implies that the ratio of these cells likely has an impact on regenerative outcome. Our results demonstrate that long ANAs have higher levels of senescence markers as well as an increased percentage of Schwann cells expressing senescence markers (of the total Schwann cell number) compared to short ANAs. This relationship suggests that the ratio of Schwann cells expressing markers of senescence (p16) is directly related to axonal growth. In addition, as a much greater accumulation of senescence markers and cells developed in long versus short ANAs, this result strongly suggests that graft length is a dependent variable affecting accumulation of cells expressing stress and senescence markers.

To confirm that the ANA environment was causal to axonal growth arrest, we directly assessed the ability of neurons near the time of axonal arrest to extend neurites. Neurons regenerated axons for an extended period (6 weeks) after replacement of the local environment with isografts. In addition, neurons harvested near the time of axonal growth arrest also extended longer neurites than naive neurons. While the neurons likely extended longer neurites than naive neurons due to injury ''conditioning,''[67,68] these results indicate that neurons are capable of growing across a long distance (such as a long construct) if provided a permissive growth environment. However, the status of neurons, including their gene profile and expression of senescence markers, was not performed in the present work, limiting our full knowledge of their axonal regenerative capabilities.

Overall, these studies establish a relationship where increased stromal cells (fibronectin$^+$/S100β^-/CD68$^-$) and the ratio of p16$^+$ Schwann cells (S100β^+) precede axonal growth arrest in long ANAs. As such, these studies suggest that these cells may play a role in the development of the deleterious environment within long ANAs. Future studies will directly assess the role of subpopulations of stromal cells and Schwann cells expressing senescent markers on axonal regeneration to establish a causal relationship.

Conclusions

This study demonstrates that axonal growth arrest occurs in long ANAs 4–6 weeks after repair, which is associated with repopulation of the graft with neural support cells and an accumulation of cellular senescence markers before arrest. We also show that expression of senescence-associated markers is significantly elevated in long ANAs relative to short ANAs, where axonal regeneration is successfully facilitated across the graft. In addition, the percentage of stromal cells (fibronectin$^+$/S100β^-/CD68$^-$) and p16$^+$ Schwann cells (S100β^+) is increased in long ANAs compared to short ANAs. Finally, this study demonstrates that the long ANA environment (as opposed to the longer distance axons must grow) is a primary cause of the poor regenerative outcome.

Acknowledgments

This work was supported in part by the National Institute of Neurological Disorders and Stroke of the National Institutes of Health under award number R01 NS086773 and the American Foundation for Surgery of the Hand award number 133987. Imaging and lentivirus in this study were supported by the Alafi Neuroimaging Laboratory, the Hope Center for Neurological Disorders, and the National Institute of Neurological Disorders and Stroke of the National Institutes of Health under award number P30 NS057105 to the Washington University. Salary support was provided in part by the Barnes-Jewish Hospital Foundation for Louis Poppler and Matthew Wood and the National Institutes of Health under award number 5 R01 CA151518 and the American Cancer Society Research Scholar Award for Sheila Stewart. The content is solely the responsibility of the authors and does not necessarily represent the official views of the National Institutes of Health or Washington University.

Disclosure Statement

No competing financial interests exist.

References

1. Noble, J., Munro, C.A., Prasad, V.S., and Midha, R. Analysis of upper and lower extremity peripheral nerve injuries in a population of patients with multiple injuries. J Trauma **45,** 116, 1998.
2. Mackinnon, S.E. Surgical management of the peripheral nerve gap. Clin Plast Surg **16,** 587, 1989.
3. Whitlock, E.L., Tuffaha, S.H., Luciano, J.P., Yan, Y., Hunter, D.A., Magill, C.K., Moore, A.M., Tong, A.Y., Mackinnon, S.E., and Borschel, G.H. Processed allografts and type I collagen conduits for repair of peripheral nerve gaps. Muscle Nerve **39,** 787, 2009.
4. Moore, A.M., MacEwan, M., Santosa, K.B., Chenard, K.E., Ray, W.Z., Hunter, D.A., Mackinnon, S.E., and Johnson, P.J. Acellular nerve allografts in peripheral nerve regeneration: a comparative study. Muscle Nerve **44,** 221, 2011.
5. Saheb-Al-Zamani, M., Yan, Y., Farber, S.J., Hunter, D.A., Newton, P., Wood, M.D., Stewart, S.A., Johnson, P.J., and Mackinnon, S.E. Limited regeneration in long acellular nerve allografts is associated with increased Schwann cell senescence. Exp Neurol **247,** 165, 2013.
6. Nadim, W., Anderson, P.N., and Turmaine, M. The role of Schwann cells and basal lamina tubes in the regeneration of axons through long lengths of freeze-killed nerve grafts. Neuropathol Appl Neurobiol **16,** 411, 1990.
7. Slegtenhorst, B.R., Dor, F.J., Elkhal, A., Rodriguez, H., Yang, X., Edtinger, K., Quante, M., Chong, A.S., and

Tullius, S.G. Mechanisms and consequences of injury and repair in older organ transplants. Transplantation **97,** 1091, 2014.
8. Nogueira, V., Park, Y., Chen, C.C., Xu, P.Z., Chen, M.L., Tonic, I., Unterman, T., and Hay, N. Akt determines replicative senescence and oxidative or oncogenic premature senescence and sensitizes cells to oxidative apoptosis. Cancer Cell **14,** 458, 2008.
9. Barascu, A., Le Chalony, C., Pennarun, G., Genet, D., Imam, N., Lopez, B., and Bertrand, P. Oxidative stress induces an ATM-independent senescence pathway through p38 MAPK-mediated lamin B1 accumulation. EMBO J **31,** 1080, 2012.
10. Chen, Q.M., Prowse, K.R., Tu, V.C., Purdom, S., and Linskens, M.H. Uncoupling the senescent phenotype from telomere shortening in hydrogen peroxide-treated fibroblasts. Exp Cell Res **265,** 294, 2001.
11. Parrinello, S., Samper, E., Krtolica, A., Goldstein, J., Melov, S., and Campisi, J. Oxygen sensitivity severely limits the replicative lifespan of murine fibroblasts. Nat Cell Biol **5,** 741, 2003.
12. Sindrilaru, A., Peters, T., Wieschalka, S., Baican, C., Baican, A., Peter, H., Hainzl, A., Schatz, S., Qi, Y., Schlecht, A., Weiss, J.M., Wlaschek, M., Sunderkotter, C., and Scharffetter-Kochanek, K. An unrestrained proinflammatory M1 macrophage population induced by iron impairs wound healing in humans and mice. J Clin Invest **121,** 985, 2011.
13. van Deursen, J.M. The role of senescent cells in ageing. Nature **509,** 439, 2014.
14. Pazolli, E., and Stewart, S.A. Senescence: the good the bad and the dysfunctional. Curr Opin Genet Dev **18,** 42, 2008.
15. Coppe, J.P., Desprez, P.Y., Krtolica, A., and Campisi, J. The senescence-associated secretory phenotype: the dark side of tumor suppression. Annu Rev Pathol **5,** 99, 2010.
16. Campisi, J. Aging, cellular senescence, and cancer. Annu Rev Physiol **75,** 685, 2013.
17. Barker, C.E., Ali, S., O'Boyle, G., and Kirby, J.A. Transplantation and inflammation: implications for the modification of chemokine function. Immunology **143,** 138, 2014.
18. Pazolli, E., Luo, X., Brehm, S., Carbery, K., Chung, J.J., Prior, J.L., Doherty, J., Demehri, S., Salavaggione, L., Piwnica-Worms, D., and Stewart, S.A. Senescent stromal-derived osteopontin promotes preneoplastic cell growth. Cancer Res **69,** 1230, 2009.
19. Alspach, E., Flanagan, K.C., Luo, X., Ruhland, M.K., Huang, H., Pazolli, E., Donlin, M.J., Marsh, T., Piwnica-Worms, D., Monahan, J., Novack, D.V., McAllister, S.S., and Stewart, S.A. p38MAPK plays a crucial role in stromal-mediated tumorigenesis. Cancer Discov **4,** 716, 2014.
20. Ruhland, M.K., Coussens, L.M., and Stewart, S.A. Senescence and cancer: an evolving inflammatory paradox. Biochim Biophys Acta **1865,** 14, 2016.
21. Baker, D.J., Wijshake, T., Tchkonia, T., LeBrasseur, N.K., Childs, B.G., van de Sluis, B., Kirkland, J.L., and van Deursen, J.M. Clearance of p16Ink4a-positive senescent cells delays ageing-associated disorders. Nature **479,** 232, 2011.
22. Baker, D.J., Childs, B.G., Durik, M., Wijers, M.E., Sieben, C.J., Zhong, J., Saltness, R.A., Jeganathan, K.B., Verzosa, G.C., Pezeshki, A., Khazaie, K., Miller, J.D., and van Deursen, J.M. Naturally occurring p16(Ink4a)-positive cells shorten healthy lifespan. Nature **530,** 184, 2016.
23. Demaria, M., Ohtani, N., Youssef, S.A., Rodier, F., Toussaint, W., Mitchell, J.R., Laberge, R.M., Vijg, J., Van Steeg, H., Dolle, M.E., Hoeijmakers, J.H., de Bruin, A., Hara, E., and Campisi, J. An essential role for senescent cells in optimal wound healing through secretion of PDGF-AA. Dev Cell **31,** 722, 2014.
24. Brushart, T. Nerve Repair, 1st ed. New York, NY: Oxford Press, 2011.
25. Bunge, R.P. Expanding roles for the Schwann cell: ensheathment, myelination, trophism and regeneration. Curr Opin Neurobiol **3,** 805, 1993.
26. Bunge, R.P. The role of the Schwann cell in trophic support and regeneration. J Neurol **242,** S19, 1994.
27. Bixby, J.L., Lilien, J., and Reichardt, L.F. Identification of the major proteins that promote neuronal process outgrowth on Schwann cells in vitro. J Cell Biol **107,** 353, 1988.
28. Wood, M.D., and Mackinnon, S.E. Pathways regulating modality-specific axonal regeneration in peripheral nerve. Exp Neurol **265,** 171, 2015.
29. Gonzalez-Perez, F., Udina, E., and Navarro, X. Extracellular matrix components in peripheral nerve regeneration. Int Rev Neurobiol **108,** 257, 2013.
30. Pola, R., Aprahamian, T.R., Bosch-Marce, M., Curry, C., Gaetani, E., Flex, A., Smith, R.C., Isner, J.M., and Losordo, D.W. Age-dependent VEGF expression and intraneural neovascularization during regeneration of peripheral nerves. Neurobiol Aging **25,** 1361, 2004.
31. Pestronk, A., Drachman, D.B., and Griffin, J.W. Effects of aging on nerve sprouting and regeneration. Exp Neurol **70,** 65, 1980.
32. Painter, M.W., Brosius Lutz, A., Cheng, Y.C., Latremoliere, A., Duong, K., Miller, C.M., Posada, S., Cobos, E.J., Zhang, A.X., Wagers, A.J., Havton, L.A., Barres, B., Omura, T., and Woolf, C.J. Diminished Schwann cell repair responses underlie age-associated impaired axonal regeneration. Neuron **83,** 331, 2014.
33. Moore, A.M., Borschel, G.H., Santosa, K.A., Flagg, E.R., Tong, A.Y., Kasukurthi, R., Newton, P., Yan, Y., Hunter, D.A., Johnson, P.J., and Mackinnon, S.E. A transgenic rat expressing green fluorescent protein (GFP) in peripheral nerves provides a new hindlimb model for the study of nerve injury and regeneration. J Neurosci Methods **204,** 19, 2012.
34. Hoben, G., Yan, Y., Iyer, N., Newton, P., Hunter, D.A., Moore, A.M., Sakiyama-Elbert, S.E., Wood, M.D., and Mackinnon, S.E. Comparison of acellular nerve allograft modification with Schwann cells or VEGF. Hand (N Y) **10,** 396, 2015.
35. Wood, M.D., Kemp, S.W., Liu, E.H., Szynkaruk, M., Gordon, T., and Borschel, G.H. Rat-derived processed nerve allografts support more axon regeneration in rat than human-derived processed nerve xenografts. J Biomed Mater Res A **102,** 1085, 2014.
36. Hudson, T.W., Liu, S.Y., and Schmidt, C.E. Engineering an improved acellular nerve graft via optimized chemical processing. Tissue Eng **10,** 1346, 2004.
37. Hudson, T.W., Zawko, S., Deister, C., Lundy, S., Hu, C.Y., Lee, K., and Schmidt, C.E. Optimized acellular nerve graft is immunologically tolerated and supports regeneration. Tissue Eng **10,** 1641, 2004.
38. Sondell, M., Lundborg, G., and Kanje, M. Regeneration of the rat sciatic nerve into allografts made acellular through chemical extraction. Brain Res **795,** 44, 1998.
39. Marquardt, L.M., Ee, X., Iyer, N., Hunter, D., Mackinnon, S.E., Wood, M.D., and Sakiyama-Elbert, S.E. Finely tuned temporal and spatial delivery of GDNF promotes enhanced nerve regeneration in a long nerve defect model. Tissue Eng Part A **21,** 2852, 2015.

40. Hunter, D.A., Moradzadeh, A., Whitlock, E.L., Brenner, M.J., Myckatyn, T.M., Wei, C.H., Tung, T.H., and Mackinnon, S.E. Binary imaging analysis for comprehensive quantitative histomorphometry of peripheral nerve. J Neurosci Methods **166,** 116, 2007.
41. Edelstein, A., Amodaj, N., Hoover, K., Vale, R., and Stuurman, N. Computer control of microscopes using μManager. Curr Protoc Mol Biol Chapter 14, Unit14.20, 2010.
42. Schneider, C.A., Rasband, W.S., and Eliceiri, K.W. NIH Image to ImageJ: 25 years of image analysis. Nat Methods **9,** 671, 2012.
43. Raff, M.C., Abney, E., Brockes, J.P., and Hornby-Smith, A. Schwann cell growth factors. Cell **15,** 813, 1978.
44. Brockes, J.P., and Raff, M.C. Studies on cultured rat Schwann cells. II. Comparison with a rat Schwann cell line. In Vitro **15,** 772, 1979.
45. Wu-Fienberg, Y., Moore, A.M., Marquardt, L.M., Newton, P., Johnson, P.J., Mackinnon, S.E., Sakiyama-Elbert, S.E., and Wood, M.D. Viral transduction of primary Schwann cells using a Cre-lox system to regulate GDNF expression. Biotechnol Bioeng **111,** 1886, 2014.
46. Berthold, C.H., Lugnegard, H., and Rydmark, M. Ultrastructural morphometric studies on regeneration of the lateral sural cutaneous nerve in the white rat after transection of the sciatic nerve. Scand J Plast Reconstr Surg Suppl **20,** 1, 1984.
47. Morris, J.H., Hudson, A.R., and Weddell, G. A study of degeneration and regeneration in the divided rat sciatic nerve based on electron microscopy. IV. Changes in fascicular microtopography, perineurium and endoneurial fibroblasts. Z Zellforsch Mikrosk Anat **124,** 165, 1972.
48. Salonen, V., Aho, H., Roytta, M., and Peltonen, J. Quantitation of Schwann cells and endoneurial fibroblast-like cells after experimental nerve trauma. Acta Neuropathol **75,** 331, 1988.
49. Schubert, T., and Friede, R.L. The role of endoneurial fibroblasts in myelin degradation. J Neuropathol Exp Neurol **40,** 134, 1981.
50. Parrinello, S., Napoli, I., Ribeiro, S., Wingfield Digby, P., Fedorova, M., Parkinson, D.B., Doddrell, R.D., Nakayama, M., Adams, R.H., and Lloyd, A.C. EphB signaling directs peripheral nerve regeneration through Sox2-dependent Schwann cell sorting. Cell **143,** 145, 2010.
51. Kalluri, R., and Zeisberg, M. Fibroblasts in cancer. Nat Rev Cancer **6,** 392, 2006.
52. Dimri, G.P., Lee, X., Basile, G., Acosta, M., Scott, G., Roskelley, C., Medrano, E.E., Linskens, M., Rubelj, I., Pereira-Smith, O., *et al.* A biomarker that identifies senescent human cells in culture and in aging skin in vivo. Proc Natl Acad Sci U S A **92,** 9363, 1995.
53. Bodnar, A.G., Ouellette, M., Frolkis, M., Holt, S.E., Chiu, C.P., Morin, G.B., Harley, C.B., Shay, J.W., Lichtsteiner, S., and Wright, W.E. Extension of life-span by introduction of telomerase into normal human cells. Science **279,** 349, 1998.
54. Vaziri, H., and Benchimol, S. Reconstitution of telomerase activity in normal human cells leads to elongation of telomeres and extended replicative life span. Curr Biol **8,** 279, 1998.
55. Itahana, K., Campisi, J., and Dimri, G.P. Methods to detect biomarkers of cellular senescence: the senescence-associated beta-galactosidase assay. Methods Mol Biol **371,** 21, 2007.
56. Moore, A.M., Kasukurthi, R., Magill, C.K., Farhadi, H.F., Borschel, G.H., and Mackinnon, S.E. Limitations of conduits in peripheral nerve repairs. Hand (N Y) **4,** 180, 2009.
57. Szynkaruk, M., Kemp, S.W., Wood, M.D., Gordon, T., and Borschel, G.H. Experimental and clinical evidence for use of decellularized nerve allografts in peripheral nerve gap reconstruction. Tissue Eng Part B Rev **19,** 83, 2013.
58. Zalewski, A.A., and Gulati, A.K. Evaluation of histocompatibility as a factor in the repair of nerve with a frozen nerve allograft. J Neurosurg **56,** 550, 1982.
59. Levi, A.D., Evans, P.J., Mackinnon, S.E., and Bunge, R.P. Cold storage of peripheral nerves: an in vitro assay of cell viability and function. Glia **10,** 121, 1994.
60. Gulati, A.K., and Cole, G.P. Nerve graft immunogenicity as a factor determining axonal regeneration in the rat. J Neurosurg **72,** 114, 1990.
61. Fox, I.K., Jaramillo, A., Hunter, D.A., Rickman, S.R., Mohanakumar, T., and Mackinnon, S.E. Prolonged cold-preservation of nerve allografts. Muscle Nerve **31,** 59, 2005.
62. Gulati, A.K., and Cole, G.P. Immunogenicity and regenerative potential of acellular nerve allografts to repair peripheral nerve in rats and rabbits. Acta Neurochir (Wien) **126,** 158, 1994.
63. Mackinnon, S.E., Hudson, A.R., Falk, R.E., Kline, D., and Hunter, D. Peripheral nerve allograft: an assessment of regeneration across pretreated nerve allografts. Neurosurgery **15,** 690, 1984.
64. Anderson, P.N., Nadim, W., and Turmaine, M. Schwann cell migration through freeze-killed peripheral nerve grafts without accompanying axons. Acta Neuropathol **82,** 193, 1991.
65. Campbell, G., Anderson, P.N., Turmaine, M., and Lieberman, A.R. GAP-43 in the axons of mammalian CNS neurons regenerating into peripheral nerve grafts. Exp Brain Res **87,** 67, 1991.
66. Salmenpera, P., Kankuri, E., Bizik, J., Siren, V., Virtanen, I., Takahashi, S., Leiss, M., Fassler, R., and Vaheri, A. Formation and activation of fibroblast spheroids depend on fibronectin-integrin interaction. Exp Cell Res **314,** 3444, 2008.
67. McQuarrie, I.G., Grafstein, B., and Gershon, M.D. Axonal regeneration in the rat sciatic nerve: effect of a conditioning lesion and of dbcAMP. Brain Res **132,** 443, 1977.
68. Bisby, M.A., and Pollock, B. Increased regeneration rate in peripheral nerve axons following double lesions: enhancement of the conditioning lesion phenomenon. J Neurobiol **14,** 467, 1983.

Address correspondence to:
Matthew D. Wood, PhD
Division of Plastic and Reconstructive Surgery
Department of Surgery
Washington University School of Medicine
Campus Box 8238
660 South Euclid Avenue
St. Louis, MO 63110

E-mail: woodm@wudosis.wustl.edu

Received: January 5, 2016
Accepted: June 9, 2016
Online Publication Date: July 1, 2016